The role of titanium in TiO_2:SiO_2 mixed sol-gels: an x-ray and neutron diffraction study

1997 J. Phys.: Condens. Matter 9 4001

(http://iopscience.iop.org/0953-8984/9/20/001)

J. Phys.: Condens. Matter **9** (1997) 4001–4016. Printed in the UK PII: S0953-8984(97)79736-4

The role of titanium in TiO_2:SiO_2 mixed sol-gels: an x-ray and neutron diffraction study

J S Rigden, J K Walters†, P J Dirken, M E Smith, G Bushnell-Wye‡, W S Howells§ and R J Newport‖

Physics Laboratory, The University, Canterbury, CT2 7NR, UK

Received 21 November 1996

Abstract. Conventional transmission and shallow-angle x-ray diffraction, together with complementary high real-space resolution neutron diffraction data, are used to reveal details of the effect of adding titania to a silica-based sol-gel. A direct observation of the Ti–O correlation has been possible. At Ti contents low enough to ensure atomic homogeneity, the data are consistent with the fourfold oxygen coordination around the metal site derived from NMR spectra. Even at these low concentrations the nature of the silica network is shown to have been affected significantly, with bondlength distributions being narrowed, and with an increased level of Si–OH indicating a qualitative change in the mesoscopic structure associated with interfacial surfaces. Data from a sample having a Ti content high enough to bring about phase separation is also presented. The shallow-angle-of-incidence x-ray diffraction method is used to provide information on the differences in structure between 'bulk' materials and those deposited as spun thin films; the data suggest an increased level of disorder in the thin films.

1. Introduction

Mixed silica:metal-oxide materials are of significant technological importance. Silica glasses with a few mol% TiO_2 are used as ultra-low thermal expansion (ULE) glasses [1] and mixed titanium:silicon oxides are important as catalysts and catalytic support materials [2]. In the optical industry they can be produced as anti-reflective thin-film coatings, with tailored refractive indices. The properties of titania:silica binaries, however, are strongly dependent on their chemical composition, homogeneity and texture. Sol-gel synthesis, based on hydrolysis of metal alkoxide precursors, and subsequent condensation, is a relatively new method that combines atomic level mixing with a high degree of porosity. Ti and Si alkoxides have very different hydrolysis rates that can mean phase separation occurs as Ti-rich and Si-rich regions form. ^{17}O NMR has confirmed that atomic mixing occurs in such glasses by revealing the presence of Ti–O–Si bonds [3, 4]; in contrast, OTi_3 and OTi_4 features in the NMR spectra [5] of glasses with higher TiO_2 content ($\sim$41 mol%) indicate that they are phase separated.

Although much work exists on the sol-gel process, details of the atomic-scale structure remain elusive; this problem may usefully be addressed using advanced spectroscopic and

† Present address: Department of Physics and Astronomy, University College London, Gower Street, London, WC1E 6BT, UK.

‡ Daresbury Laboratory, Daresbury, Warrington, WA4 4AD, UK.

§ Neutron Division, Rutherford Appleton Laboratory, Chilton, Didcot, OX11 0QX, UK.

‖ Author to whom correspondence should be addressed.

0953-8984/97/204001+16$19.50

scattering techniques. Silica and silica:titania binaries have been studied in their crystalline phases using x-ray diffraction [6, 7], but relatively little work has been undertaken on the gels in their amorphous state [8]. Transmission x-ray or neutron diffraction can reveal structural information averaged over an entire sample, and is therefore a useful method for studying bulk material. However, conventional techniques cannot be used to study thin films or coatings, due to the difficulty in separating the signal arising from the film from that of the substrate. Shallow angle x-ray diffraction, where penetration depths are lessened by reducing the incident angle of radiation onto the film, is a relatively new technique which can enable structural information from a thin film to be isolated. We have undertaken x-ray (both in shallow angle and transmission geometry) and neutron diffraction experiments on pure silica and three SiO_2:TiO_2 sol-gel binaries with titanium content varying from 0 to ∼5 at%: the silica system, two at Ti levels low enough to ensure no phase separation and a fourth sample with sufficient Ti to induce phase separation.

2. Experimental details: sample preparation

The SiO_2–TiO_2 mixed gels were prepared by hydrolysis of titanium *n*-propoxide ($Ti(OPr^n)_4$) and tetraethoxy orthosilicate (TEOS). Four sol-gel glasses were prepared with water and propanol mixtures in the approximate ratios 1:2:7.5, with varying titania contents. Sample 1, labelled 'pure silica', contained no titania, samples 2 and 3 contained 8 and 18 mol% titania (0.4 and 0.84 at% Ti), respectively, and were labelled '8 mol% titania' and '18 mol% titania', respectively. Sample 4 contained very high titania levels (41 mol% ≡4.9 at%) and was in the compositional range for which phase separation was predicted to occur; this sample was labelled '41 mol% titania'. It must be noted that all four samples contained substantial residual amounts of volatile alcohols. Full details of the sample preparation and characterization are given elsewhere [4, 8, 9]. Table 1 shows the compositional information, determined by a combination of standard chemical analysis and the weight loss, including mass and electron densities. It is immediately evident that the sample labelled '41 mol% titania' was compositionally very different from the samples which were expected to be atomically mixed. Whilst the other samples maintained a hydrogen:carbon ratio of ∼2.7:1, the H:C ratio for sample 4 has risen to ∼6:1, with much less carbon but much more oxygen held in the system.

Table 1. Compositional information for the four samples studied.

Sample	Composition (at%)					Density (g cm^{-3} {atoms $Å^{-3}$})	Electrons (per $Å^3$)
	Ti	Si	O	C	H		
1 Pure SiO_2	0.0	4.0	16.2	21.6	58.6	2.25 {0.20}	0.736
2 8 mol% titania, SiO_2:TiO_2	0.4	4.7	19.7	20.2	55.5	2.45 {0.19}	0.789
3 18 mol% titania, SiO_2:TiO_2	0.84	3.8	17.0	21.0	57.3	2.65 {0.22}	0.856
4 41 mol% titania, SiO_2:TiO_2	4.9	7.0	38.2	7.0	42.7	3.10 {0.16}	0.954

The silica sol-gel and the two lower titanium content mixed gels, were used to produce thin films by the *spin coating* method [1]; the '41 mol% titania' sample could not be used to create a thin film as it was not possible to produce a uniform precursor sol. An excess

of liquid is dropped onto the surface of the substrate, and then the sample is rotated at low speed so that the liquid flows radially outwards, driven by centripetal force. Surplus liquid flows to the edge of the substrate and drips off. As the film thins, the rate of removal of liquid slows down as the viscosity increases; in the final stages most of the thinning occurs by evaporation of volatiles [10]. This method produces a very uniformly thin coating, and the process may be repeated several times to build up a thicker film or, for example, to produce layers with slightly differing qualities. In the present case, six layers of film were deposited from the same stock mixture to produce a film ~ 1 μm thick on a polished silicon wafer.

Although the underlying physics and chemistry that govern growth and gelation are the same for films and bulk sol-gels, several factors in the evolution of thin films mean that, structurally, the two forms may be quite different [1]. In bulk systems evaporation usually occurs after gelation, whereas in thin films the deposition and evaporation processes occur simultaneously, and this results in a competition between compaction of the structure caused by evaporation and the stiffening (and therefore resistance to compaction) of the material caused by the structural condensation process. The short duration of deposition and evaporation/drying in thin films means that considerably less crosslinking occurs than in bulk gels, which generally results in more compact dried structures; this is particularly true for films made by spinning methods. Also, thin films are constrained by their geometry, and the continued shrinking causes stresses. It is likely, therefore, that the rapid gelation of thin films will result in a more disordered material than in the bulk with a lower concentration of volatiles.

3. Experimental details: diffraction

The neutron data presented here were collected using the LAD diffractometer at the ISIS pulsed neutron facility at the Rutherford Appleton Laboratory (UK) [11] which has a wide dynamic range available ($\sim$0.2–50 Å^{-1}), and hence offers a high resolution in real space since $\Delta r \sim 2\pi/Q_{max} = 0.13$ Å and in addition minimizes the residual effects of truncation errors. In performing a diffraction experiment, the quantity we wish to obtain is the structure factor $S(Q)$, where, for an amorphous material (i.e. an isotropic scatterer) [12],

$$S(Q) = 1 + \frac{4\pi\rho}{Q}\int_0^\infty r\,\mathrm{d}r\,[g(r) - 1]\sin(Qr) \tag{1}$$

in which ρ is the average number density of atoms in the material, $Q = |\boldsymbol{Q}| = (4\pi/\lambda)\sin\theta$ is the wave-vector transfer associated with the diffraction experiment, 2θ is the scattering angle and λ is the neutron wavelength; $g(r)$ is the pair-correlation function, which is a measure of the atomic density at a distance r from a given atom at the origin. The pair-correlation function may be obtained by Fourier transformation of the structure factor, which is directly related to the measured neutron scattering intensity.

In a multicomponent system there are contributions to the total structure factor from each atom-type pair (e.g. Ti–O, Si–O, C–O, O–O, ...) such that the total structure factor $F(Q)$ is given by

$$F(Q) = \sum_\alpha c_\alpha^2 b_\alpha^2 + \sum_{\alpha\beta} c_\alpha b_\alpha c_\beta b_\beta [S_{\alpha\beta}(Q) - 1] \tag{2}$$

where c_α and c_β are the atomic fractions, b_α and b_β are the neutron scattering lengths, respectively, of elements α and β, and $S_{\alpha\beta}(Q)$ is the partial structure factor. The first summation represents the 'self-' or 'single-atom' scattering, while the second corresponds

to the 'interference' or 'distinct' scattering and contains the basic information on atomic correlations. Fourier transformation leads to the total pair-correlation function $G(r)$:

$$G(r) = \frac{\sum_{\alpha\beta} c_\alpha c_\beta b_\alpha b_\beta [g_{\alpha\beta}(r) - 1]}{\sum_\alpha c_\alpha^2 b_\alpha^2} + 1 \tag{3}$$

where $g_{\alpha\beta}(r)$ represent the partial terms in $G(r)$. Note that the X–H terms, where X = C or O, and the X–Ti terms, where X=O, are negative due to the π phase shift experienced by the neutron on scattering from H and Ti: features in the pair correlation function corresponding to Ti–O, for example, will therefore appear as troughs rather than peaks. (Note, however, that it also must follow that all H–H and Ti–Ti pairwise terms, including second-neighbour features such as H–C–H, will be associated with positive-going peaks [12].) Although, in principle, all $g_{\alpha\beta}(r)$ are embedded within $G(r)$, the coefficients associated with pairs of minority species such as Ti–Ti will be vanishingly small, and others such as H–H (e.g. that associated with molecular hydrogen) may reasonably be ignored on chemical grounds. Whilst it is meaningful to discuss the statistical accuracy of $F(Q)$s, where error bars on individual points were determined to be $\pm 1\%$ at their worst, the 'errors' associated with $G(r)$ are not so tractable given the intervening Fourier transformation; we have adopted the usual approach of limiting our discussion to those features that remain despite variations in the inversion process (e.g. the value of Q_{max} used, the nature of any windowing function applied, the use of indirect inversion methods such as those based on a Monte Carlo approach). Apart from very low values of r, where Fourier transformation effects are at their most significant, peak positions in $G(r)$ tend to be reliable to ± 0.04 and ± 0.06–0.08 Å for neutron and x-ray diffraction data, respectively, the corresponding figures for peak areas are $\sim$15 and 20–25%. Before obtaining the neutron $F(Q)$ several corrections need to be applied to the data, the major ones being for background, container and multiple scattering, attenuation and the effects of inelastic scattering. Full details of these and their effect on data from hydrogenated materials may be found elsewhere [12–14].

Both transmission and shallow-angle x-ray diffraction measurements were carried out on Station 9.1 at the Synchrotron Radiation Source at the Daresbury Laboratory (UK). The intrinsically highly-parallel nature of the beam provided by a synchrotron source is of advantage over conventional focused laboratory x-ray sources for the shallow-angle technique in that the associated geometric aberration effects are avoided [15]. Further, the high intensity beam provided by a synchrotron source is necessary for the relatively weak scattering from the small volume of amorphous material sampled in the shallow-angle geometry; also the availability of hard x-rays allows a relatively wide dynamic data range (potentially up to $\sim$20–24 Å^{-1}).

The shallow-angle technique was first developed by Lim and Ortiz [15], who studied polycrystalline iron oxide layers on glass substrates, i.e. sharp Bragg peaks on a diffuse Debye–Scherrer background. The method and analysis has recently been developed further [16] and used to study a variety of both amorphous and crystalline thin films. The refractive index of materials at x-ray wavelengths is less than unity, consequently, at incident angles below a critical value, α_c, total external reflection occurs. Below α_c limited penetration is achieved via the evanescent mode, and is exponentially damped: in principle sampling depths of $\sim$10 Å to $\sim$1000 Å may be achieved. Above α_c the penetration depth increases rapidly with incident angle, inversely with the wavelength of the radiation, and is limited by photoelectric absorption; it is this region where shallow-angle diffraction can be used in a practical way to isolate scattering from a thin film in its *as-deposited* state on a substrate. The conventional (transmission) x-ray diffraction arrangement [17] is modified to produce the shallow-angle configuration, as shown schematically in figure 1. The white beam from

the synchrotron source is monochromated by a channel cut crystal and proceeds through a pair of slits which define the incident beam profile; a narrow slit profile of 100 μm by 10 mm is used in shallow-angle work to limit off-sample contamination scattering from the straight through beam at the lowest incident angles, where the beam's 'footprint' will be at its largest. The sample is set at a fixed, small angle α_i to the incident x-rays. A long-slit package limits the viewed area and reduces the angular spread of scattered radiation incident on the detector and results in a resolution of $\sim$0.07. Data are collected sequentially at angles $2\theta = 2$–130°.

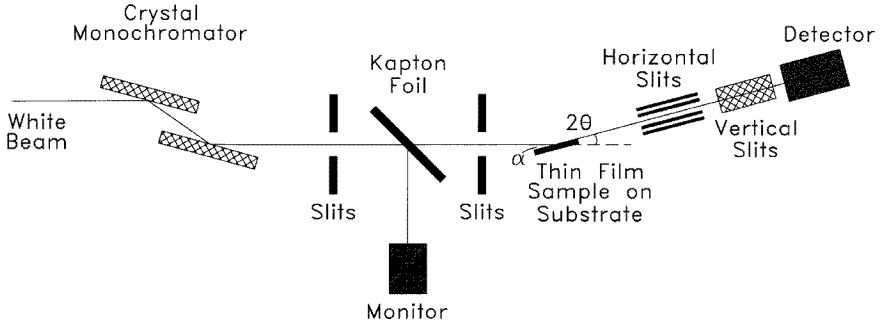

Figure 1. Schematic diagram of the shallow-angle-of-incidence x-ray diffraction method.

Preliminary data reduction for transmission diffraction [18] includes correction for dead-time losses, the polarization of the incident x-ray beam, the removal of the θ dependence resulting from the changing sample volume illuminated, the sample container and background scattering, and finally the data are corrected for sample absorption effects. For a system of N identical atoms the scattered intensity (in electron units) is given by [19]

$$\frac{I_{eu}(\boldsymbol{Q})}{N} = \sum_m f^2 + \sum_m f^2 \sum_{n \neq m} \mathrm{e}^{\boldsymbol{Q}\boldsymbol{r}_{nm}} \tag{4}$$

where f is the atomic form factor and $\boldsymbol{r}_{nm}$ is the distance vector between the positions of atoms n and m. This equation represents both the intra-atomic (self-scattering) and inter-atomic scattering (interference term) of the system. In the experimental data a third term is also collected which includes the inelastic scattering produced by the system; this can be calculated using tables [20] and removed.

When there is more than one atom type, an approximate method can be used to calculate the x-ray scattered intensity by choosing a convenient 'unit of composition', uc, for the material. We can then define an *average* scattering factor per electron [19]:

$$f_e = \frac{\sum_{uc} f_m}{\sum_{uc} Z_m} \tag{5}$$

where the sum over uc represents the weighted sum over the atoms of atomic number Z_m. The form factor for each atom type can then be approximated by $f_m = K_m f_e$, where K_m will be approximately equal to Z_m. In each case K_m will vary with scattering vector $\boldsymbol{Q}$, and the validity of this treatment depends on the error in treating K_m as an average over the entire $\boldsymbol{Q}$ range involved.

For any given displacement $\boldsymbol{r}$, the electron density averaged over all directions is given by $\rho_j(\boldsymbol{r})$ where the subscript j represents the atom type; this shows fluctuations from the average electron density of the sample ρ_e. For an amorphous material with no preferred

orientation, spherical symmetry can be assumed here, as for the entirely analogous neutron formalism, and the integral over volume may therefore be reduced to

$$\frac{I_{eu}(Q)}{N} - \sum_{uc} f_j^2 = f_e^2 \sum_{uc} K_j \int 4\pi r^2 [\rho_j(r) - \rho_e] \frac{\sin Qr}{Qr} \, \mathrm{d}r. \tag{6}$$

The left-hand side of the equation is readily obtainable from experiment and is the x-ray structure factor $S(Q)$. In practice it is not possible to measure x-ray diffraction data directly in electron units; an absolute intensity measurement is therefore obtained by scaling the data to oscillate about the theoretical self-scattering term, and hence producing $S(Q)$. Inverting this by Fourier transformation, we obtain the total pair distribution function.

Shallow-angle x-ray diffraction data cannot be treated in the same quantitative manner: basic data reduction accounts for detector dead-time, changes in incident beam current and beam polarization effects. A further correction is needed to account for the fact that the collected x-ray beam is actually scattered from the refracted beam within the sample; this produces a small shift in the measured scattering angle 2θ. More sample-specific corrections such as sample absorption and multiple scattering are not included in the reduction procedure for the shallow-angle technique; these corrections are complicated by unknown factors in the sample geometry which make it difficult to determine the actual spread of penetration depths into the sample and/or substrate and the contributions from each. This situation could be clarified somewhat if the incident x-rays did not penetrate the substrate at all; this can be achieved either by using thicker films, reducing the incident angle or increasing the incident x-ray wavelength; however, increasing λ decreases the Q-range and therefore the real-space resolution, and there is little to be gained by reducing a_i much below the detector slit resolution. Progress in the longer term is likely to depend on the use of indirect data-reduction tools based on Monte Carlo methods. Subtraction of the background scattering in the shallow-angle geometry is also problematic, as there is no direct method of removing the sample and measuring the 'background' scatter. It must therefore be assumed that the background scattering may be approximated by a smooth curve and therefore removed, along with the atomic form factor, by fitting a Chebyshev polynomial through the data. While this method produces an 'interference function' which shows the same peak positions as would be derived by following standard procedures for transmission geometry data, there is no practicable method of converting the data to electron units, and therefore it is not possible to produce absolute coordination numbers from the real-space information.

4. Results and discussion

4.1. Bulk samples

The $F(Q)$ and $G(r)$ spectra derived from the neutron data are shown in figures 2 and 3 respectively. The analogous spectra for transmission x-ray diffraction are shown in figures 4 and 5 (the plot is limited to a Q-range $\leqslant 10$ Å^{-1} for clarity). It is immediately apparent from the $F(Q)$ spectra that all samples are amorphous; a key observation, seen particularly clearly in the neutron case, is that, even for the lowest Ti content, there is an increase in oscillations above $Q \sim 7$ Å $^{-1}$ compared to the pure silica case, which is indicative of an increasingly well defined short/medium-range order.

Considering first the conventional x-ray diffraction data, the general shape of all four curves is the same, with only the '41 mol% titania' curve showing a large increase in the intensity of the oscillations. Since x-ray scattering results from interaction with electrons, scattering will be dominated by correlations involving heavier atoms, i.e. Si, Ti and O. It

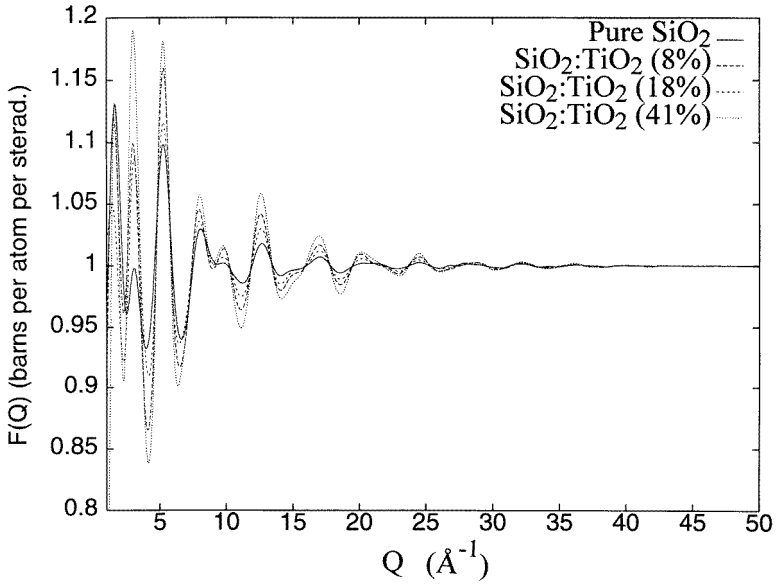

Figure 2. Total structure factors for the sol-gel samples derived from neutron diffraction as a function of mol% TiO_2 content; sample details are given in table 1 (error bars on individual points were determined to be $\pm 1\%$ at their worst).

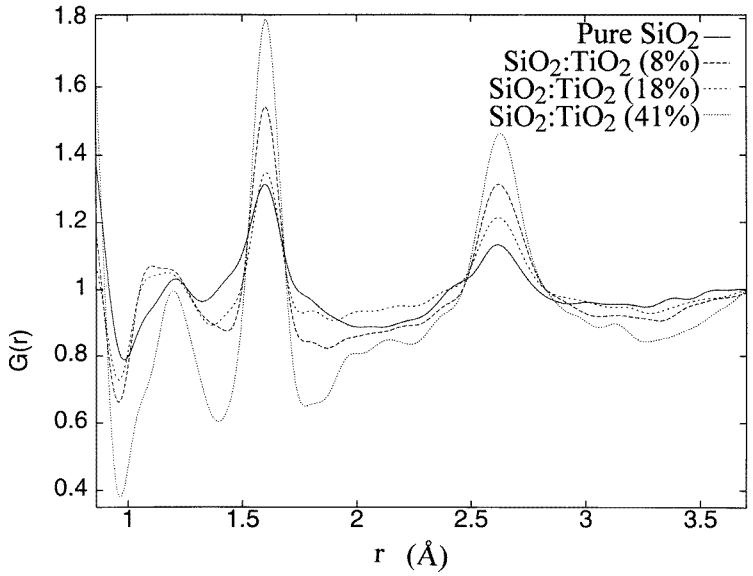

Figure 3. Pair distribution functions for the sol-gel samples derived from neutron diffraction as a function of mol% TiO_2 content (note that $G(r)$ is dimensionless, equation (3)); sample details are given in table 1.

can be seen from table 1 that samples 1 to 3 show very similar compositions with either none or only small amounts of titanium present; sample 4, however, contains significantly more titanium which has resulted in the much stronger x-ray scattering.

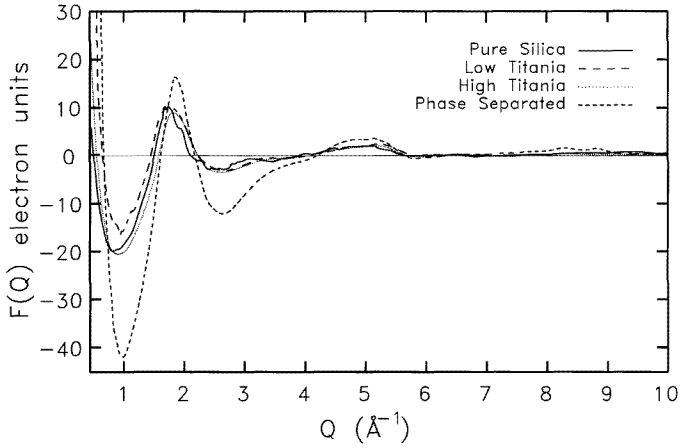

Figure 4. Total structure factors for the sol-gel samples derived from transmission x-ray diffraction as a function of mol% TiO_2 content; sample details are given in table 1.

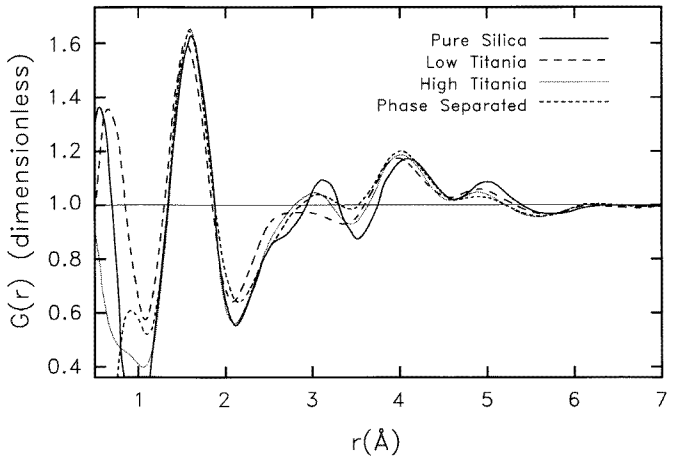

Figure 5. Pair distribution functions for the sol-gel samples derived from transmission x-ray diffraction as a function of mol% TiO_2 content; sample details are given in table 1.

Clear differences in the shape of the $G(r)$ curves for the four samples are evident, particularly in the region of the second and third neighbours. The first main peak at ∼1.6 Å shows slight differences in position, but the peaks are similar in width and height, indicating that all four samples have a very similar first-neighbour environment within the resolution of the data, and with the weighting factors involved in the pairwise terms. Since the $F(Q)$ data covered a relatively short useable dynamic range in this case (0.45–14 Å^{-1}), and a heavy windowing function [21] was used in the Fourier transform to avoid termination errors, the resolution of the real-space data is relatively low; all correlations between ∼1.4 and 1.9 Å, therefore, are contained within the first peak. This region is expected to include correlations from Si–O at 1.61 Å, the short fourfold coordinated Ti–O distance at 1.82 Å (if present), and the C–O and C–C correlations at 1.43 and 1.53 Å of any residual propanol present in the sample. The low resolution of the data means that it is not possible

to distinguish between first-neighbour Si–O and Ti–O distances if the network remains fourfold coordinated; however, if phase separation occurred and regions of pure sixfold coordinated titania were formed, the longer Ti–O correlation length of 1.93 Å should be visible, resulting in a wider first peak for the '41 mol% titania' sample. Although there is a slight widening of the peak visible in the '41 mol% titania' sample, it is not clear whether this is statistically significant. Differences are visible in the $G(r)$ data between ∼2.2 and 3.4 Å, however, corresponding to the O–Si–O, O–Ti–O, Si–O–Si, Si–O–Ti or Ti–O–Ti correlations, tabulated in table 2, for which the x-ray weights are well conditioned (see table 3). Whilst the interatomic distances for fourfold coordinated silica and sixfold coordinated titania are known, there is some uncertainty concerning the distances within an atomically mixed silica:titania amorphous network. The distortion which will be produced when a titanium atom with a long Ti–O distance is substituted into the silica network may result in a slight shortening of the Si–O distance or a distortion in the bond-angle distribution. The distances in table 2 were calculated assuming that bond angles and distances are the same in the atomically mixed case as in pure silica; the values will therefore only be an indication of the possible interatomic distances.

Table 2. Expected second-neighbour interatomic distances for different types of correlations.

	SiO_2 fourfold coordinated		SiO_2:TiO_2 atomically mixed		TiO_2 sixfold coordinated	
Correlation	O–Si–O	Si–O–Si	O–Ti–O	Si–O–Ti	O–Ti–O	Ti–O–Ti
Distance (Å)	2.62	3.06	∼3.0	∼3.3	2.46, 2.79	3.03

Table 3. Expected bond distances for pairwise correlations present in silica:titania sol-gels, together with the weights per atom pair associated with both the x-ray and neutron case (the weights are relative values only, having been normalized within the table to unity, and in the x-ray case they related to $Q = 0$).

Correlation	Bond distance (Å, approximate)	Neutron weight (per atom pair, relative)	X-ray weight (per atom pair, relative)
O–H	0.95	$\lvert -0.13\rvert$	0.02
C–H	1.10	$\lvert -0.14\rvert$	0.02
C–O	1.41	0.22	0.12
C–C	1.53	0.25	0.09
Si–O	1.6	0.14	0.29
Ti–O	1.8	$\lvert -0.12\rvert$	0.46
Second neighbours	>∼2.0	Positive (e.g. H–C–H) and negative (e.g. Si–O–H)	all positive

The $G(r)$ data for the 'pure silica' sample show a strong peak at 3.12 Å with a distinct shoulder at ∼2.65 Å. Despite the limited real-space resolution, the data shows clearly that correlations in this region result from two separate main interatomic distances, those of O–Si–O and Si–O–Si. The introduction of a very small amount of titanium in the 'low-titania' sample results in an immediate change in the shape of the curve with the two peaks becoming of similar intensity, but with a plateau formed between them. This observation suggests that the network has become more complex, with a range of correlations forming. This is consistent with a small number of O–Ti–O and/or Si–O–Ti bonds forming in the

network, indicating the presence of atomically mixed SiO_2:TiO_2 regions. The findings for the '18 mol% titania' sample follow this trend, with more correlations occurring at longer distances corresponding to mixed correlations at or above 3 Å, and less at the O–Si–O distance of 2.6 Å.

The sample labelled '41 mol% titania' does not appear, on averaging over the entire sample, to be structurally different from the lower titania samples. The same trend of a slight shift to longer distances is observed, but there is no clear direct evidence for O–Ti–O correlations at 2.46 and 2.79 Å as might be expected if phase separation had occurred (although the peaks do appear to be slightly wider which, given the resolution of the data, would be consistent with phase separation). It is interesting to observe the formation of a peak at ∼0.95 Å in the '41 mol% titania' sample, which is also visible in the '18 mol% titania' sample although is less intense. This peak may result from the O–H bond distance, being present in either volatiles such as ethanol, or in the main silica:titania network. Since there is little carbon in the '41 mol% titania' sample (see table 1) it is likely that the O–H groups are forming *within* the silica:titania network, and increasing in number as the amount of titanium in the sample is increased. This might suggest that O–H groups, which will act as network terminators, are acting to reduce the stresses formed by the distortion of the network at titanium sites, or are forming at the boundary between regions of phase-separated silica or titania. However, the x-ray data alone are insufficient for a definitive conclusion to be drawn.

Turning now to the neutron data, the $G(r)$ are relatively complex given the number and relative weights of pairwise terms involved, some of which are negative-going (see table 3), but are nevertheless revealing by virtue of the improved real-space resolution. Peaks at ∼1.6 Å are assigned to Si–O; Ti–O distances, observed clearly in this direct manner for the first time due to the resolution now available, appear as a dip at ∼1.8 Å.

Loshmanov *et al* [22] have also claimed to have observed the Ti–O correlation, but at ∼2 Å, using neutron diffraction. However, their dataset had a very limited dynamic range and hence poor real-space resolution ($\Delta r \sim 2\pi/Q_{max} = 0.13$ Å in this work, whereas $\Delta r \sim 0.47$ Å in their work) such that any feature associated with Ti–O could not be directly resolved from the dominant Si–O peak; an associated problem is that truncation effects arising from the Fourier transformation to $G(r)$ are severe. In addition, their data suffered from poor statistics (due to the relatively weak sources then available) and was corrected in an approximate fashion only. Nevertheless, they were able to attempt to isolate any Ti–O correlation by taking a difference between a pure SiO_2 gel and those containing TiO_2, and assigning a feature at 2 Å to Ti–O on the grounds that its amplitude increased as the TiO_2 mol% increased.

The distinction between our (direct) observation and the earlier inference is an important one: for Ti in an octahedrally bonded oxide the Ti–O bondlength is 1.91–2.01 Å (i.e. corresponding to that inferred in [22]), whereas for a fourfold oxygen coordinated tetrahedral situation the bondlength is shorter at ∼1.82 Å [4, 23] which corresponds closely to the present data. Although we observe a clear negative feature at 1.8 Å, corresponding to the Ti–O tetrahedral correlation, it is not possible to obtain a more precise bond distance, nor any reliable estimate of the coordination number, because of the likely presence of a small H–C–H second-neighbour peak, also at ∼1.8 Å. ^{17}O NMR clearly demonstrates that the configuration is closer to tetrahedral than to Ti_6–O–Si or Ti_5–O–Si [3, 4], so the Ti coordination number is most probably four on the basis of available NMR data. The present data strongly supports this conclusion. The majority of second-neighbour distances occur above ∼2 Å, with the large peak at ∼2.6 Å being the envelope of features associated with O–Si–O, O–Ti–O, etc; the neutron scattering lengths are such that these terms are

down-weighted relative to the x-ray case.

Features below ∼1.5 Å are due to some extent to residual amounts of solvent (propanol/ethanol) within the gels [3–5]. For instance, as in the x-ray case, the negative-going feature in $G(r)$ at ∼1 Å can be assigned to the O–H distance (0.95 Å), with C–H (1.1 Å, also negative) causing an asymmetry in the peak. However, it should be noted that apart from the substitution of –OH groups from the alcohol molecule for –OEt groups formed as part of the reaction process, the solvent molecule undergoes no further decomposition and their contribution to $F(Q)$ may therefore be accurately predicted. Note that the negative-going feature associated with O–H and C–H correlations is dominated by the (0.95 Å) O–H correlations. Given that there are five times as many C–H bonds as there are O–H in each solvent molecule, it follows that there must be a large number of –OH groups incorporated within the network itself for it to be an O–H correlation feature that dominates: this is true for all the samples, and confirms the interpretation of the x-ray data. Supportive experimental evidence for this comes from infrared and Raman spectroscopy measurements [24, 25] and from NMR [3, 4]. Since H necessarily acts as a network terminator (and is therefore involved in the formation of voids) the relative proportions of –OH groups in the samples is likely to be associated with macroscopic structural differences between the samples. The addition of Ti to the system is therefore seen to affect the distribution and number of –OH groups.

The high real-space resolution neutron data also show that adding Ti causes a noticeable reduction in the width of the Si–O peak, although the position is constant at 1.60 Å, which is an observation that might at first sight indicate a reduction in –OH network terminators rather than the increase suggested above, since the Si–O distance will be different in Si–O–H and Si–O–Si, and a narrower peak therefore implies less such 'mixed bonding'. However, these apparently disparate observations may be satisfactorily brought together if one assumes that the –OH group's environment is different in the Ti-containing material. To examine this effect in more detail, the Si–O peak, together with features either side, were fitted with a series of Gaussians, allowing both width and height to vary. The peak positions and full-width-at-half-maximum (FWHM) height for the Si–O peak obtained by this method are given in table 4. The FWHM decreases when Ti is incorporated into the network. This may be due in small part to the presence of the Ti–O negative feature immediately following the Si–O peak, but this effect will be relatively minor. Note that the average bond distances given in table 4 for the Si–O first and O–Si–O second neighbours (the major contribution, given the neutron weights, to the peak centred at 2.6 Å) gives a bond angle of ∼110°, consistent with a disordered tetrahedral network. Also, we may note that there is no large change to this averaged bond angle when Ti is included in the network, but it must be borne in mind that the neutron data are not well-conditioned in this context.

Table 4. Results obtained from Gaussian fitting to the neutron-derived $G(r)$; the figures in brackets in column 1 refer to the mol% of TiO_2.

	Si–O		Second neighbours	
Sample	Position (Å)	FWHM (Å)	Position (Å)	Width (Å)
Pure SiO_2	1.60	0.065	2.61	0.085
SiO_2:TiO_2(8 mol%)	1.60	0.057	2.62	0.085
SiO_2:TiO_2(18 mol%)	1.60	0.053	2.62	0.084
SiO_2:TiO_2(41 mol%)	1.60	0.057	2.62	0.083

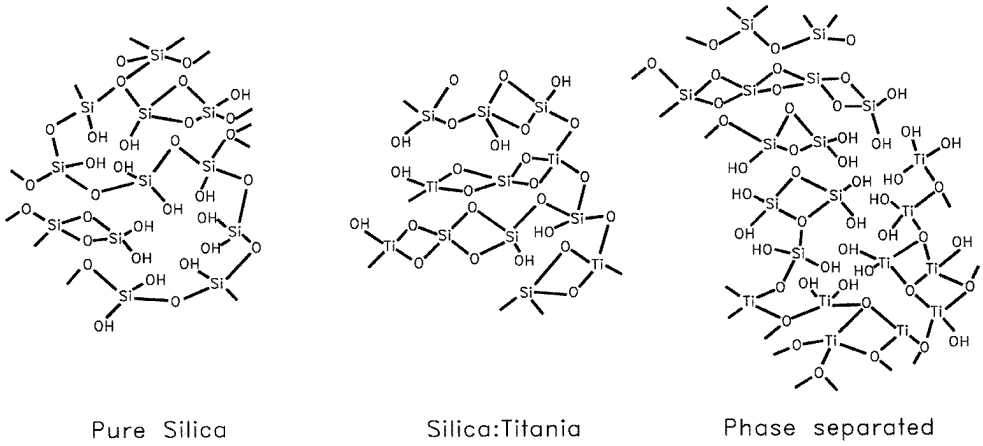

Figure 6. Schematic representation of the pure silica and the Si:Ti mixed gel network structures.

Titanium catalyses condensation processes [1], which results in the production of a more continuous network structure (for any given heat treatment, it being noted that a higher density may also be achieved by heating). It is reasonable to suppose, then, that in the samples containing Ti there should be fewer –OH groups in the bulk structure, since these are eliminated by condensation, and hence there are fewer large voids (a denser material is produced). These effects will narrow the distribution of Si–O bondlengths. However, although we do indeed observe a decrease in the width of the Si–O peak, we also see from both data sets indications of a simultaneous increase in the number of –OH groups. It is possible that the –OH reside on external/dislocation surfaces rather than on the inner surfaces of voids. In this way there will be relatively large volumes of homogeneous silica:titania network, giving rise to a narrowing of the Si–O peak, but at the same time the effect of the larger Ti atom will be to produce some distortion of the native SiO_2 tetrahedral network, thereby increasing the amount of strain: this latter effect may give rise to 'sheets' of high –OH content within the material in which the strain is relieved. A schematic representation of this effect is shown in figure 6.

In the 41 mol% titania sample where separate regions of SiO_2 and TiO_2 form, the effects mentioned above continue to be reflected. Although the sample now contains 41 mol% Ti, no further narrowing of the Si–O peak is observed. However, as has been noted already, this sample contains a much larger proportion of –OH groups. Following the same arguments as before, these cannot be on the surfaces of voids, as the structure contains very few large voids, so they must be on other 'surfaces'. The large increase in the –OH content in this sample implies that a larger surface area is available, and it is reasonable to suppose that this is a direct result of phase separation, i.e. they form an interface between the two phases. It should be noted that Ti–OH bonds were not detected by ^{17}O NMR [4], although they are intrinsically difficult to observe in this way.

4.2. Spun thin film samples

Figure 7 shows the corrected data for the three sol-gel samples after fitting and subtracting a polynomial from the data. The scattering from the samples containing titania look very similar, but the 'pure silica' sample shows a much stronger scattering across the whole Q-range. Small Bragg peaks due to the silicon substrate are visible at 6.0 and 9.5 $Å^{-1}$ (the

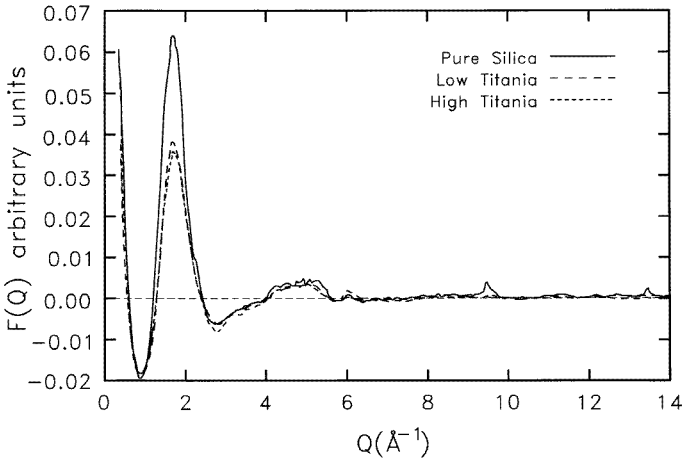

Figure 7. Total structure factors derived from shallow-angle-of-incidence x-ray diffraction from spun thin films as a function of mol% TiO_2 content.

{511} and {800}, respectively) and at 13.5 Å^{-1} in the 'pure silica' and '8 mol% titania' samples, although only the peak at ∼6 Å^{-1} appears to be present in the '18 mol% titania' sample; this is likely to be due to the fact that the higher titania film is more electron dense and therefore the incident beam is attenuated more strongly. This observation, coupled with the fact that the silicon peaks are very small, suggests that the penetration depth covered by the incident x-rays is only just greater than the thickness of the films, and so penetration into the silicon wafer is small. The sharpness of the first sol-gel peak in the 'pure silica' data at ∼1.9 Å^{-1} may, in addition, indicate contamination from an underlying residual silicon Bragg reflection.

The interference functions reveal the similarities between the scattering from all three samples after the first major peak. It is clear that the visible Bragg peaks, particularly the one at ∼6 Å^{-1}, represent a significant problem if analysis were to continue by way of conventional direct Fourier transform to a pair distribution function; their presence could lead to strong silicon correlations in $G(r)$. However, the rapid decay of the data to the asymptotic value, after the first sharp peak at ∼1.8 Å^{-1} and a small second peak at ∼4.5 Å^{-1}, indicates that all three samples show a high degree of disorder. This is demonstrated further in figure 8 where scattering from the '18 mol% titania' sample in thin-film form (shallow-angle geometry) is compared to scattering from the bulk (x-ray, transmission geometry); both data sets are at a similar stage of data reduction. Both curves are dominated by a first sharp peak primarily associated with Si–O first-neighbour correlations, but the bulk sample also shows definite second and third peaks; for the thin-film sample it is very difficult to determine any distinct higher-order correlations, although some evidence of residual structure in that region is visible. Due to the contamination by silicon Bragg reflections, and the large amount of statistical noise in the data produced by scattering from very small effective sample volumes, the information available from a Fourier transformation into real space is limited; figure 9 shows the Fourier transform of the '$F(Q)$' function for the '18 mol% titania' sample as an example of the r-space information obtainable.

The strong correlation visible at ∼1.5 Å is associated with the Si–O distance; in bulk silica the Si–O first neighbour distance is 1.61 Å; however, the silicon–oxygen distance is reduced to 1.50 Å when taken out of the confines of the silica network, for example when

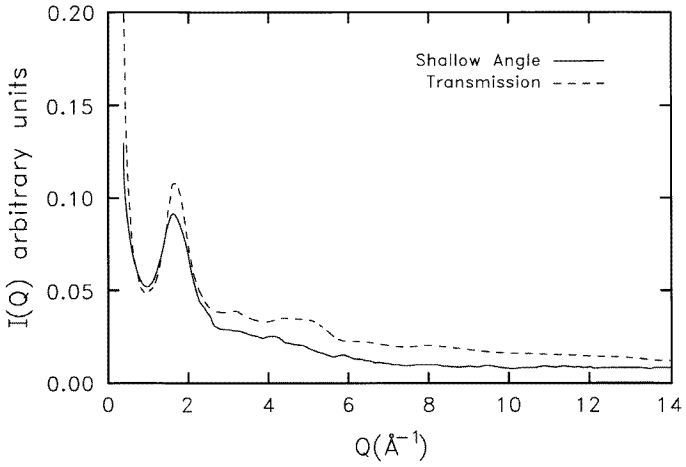

Figure 8. Comparison between the structure factors measured for sample 3 using: (*a*) conventional transmission x-ray diffraction (bulk/powder sample); and (*b*) shallow-angle-of-incidence x-ray diffraction (spun thin films).

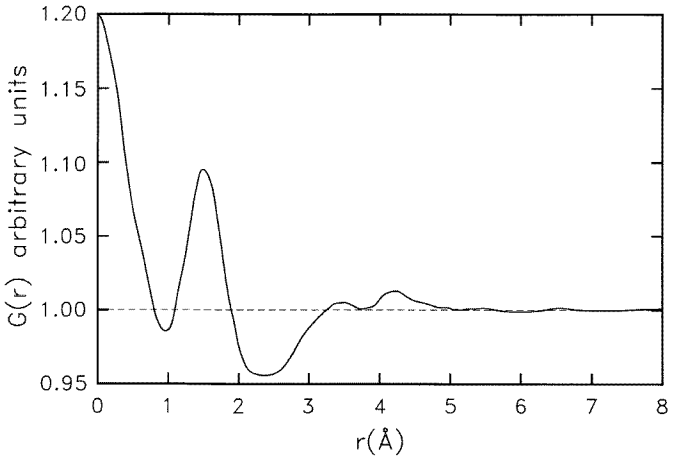

Figure 9. Fourier transform of the '$F(Q)$' derived from shallow-angle-of-incidence x-ray diffraction from sample 3.

part of an $Si(OH)_4$ unit. This may be further evidence that the silica network has become more disordered when in a thin film, and in contrast to the case for the bulk material, there are few long silicon–oxygen chains and more hydrogen atoms terminating the network. There is little order apparent in '$G(r)$' after the first main peak; in particular, interatomic distances resulting from O–Si–O (2.6 Å) and Si–O–Si (3.0 Å) bonds which are prominent in $G(r)$ data from the bulk silica:titania sol-gels are not visible here.

5. Conclusions

From these measurements it can be concluded that, in agreement with other experimental data, the sol-gel samples have a disordered tetrahedral structure in which Ti atoms are

substitutionally incorporated into the silica network at low Ti concentrations—the clearest evidence is from the x-ray data which shows an increase in the number of O–Ti–O and Ti–O–Si bonds with increasing Ti content below ∼20 mol%. For higher atomic percentages of titanium, there is no direct evidence for the existence of phase-separated areas of sixfold coordinated Ti, although this cannot be discounted; the increasing O–H coordination number in the highest titanium content sample does, however, indicate that phase separation has indeed occurred. The Ti–O correlation is clearly observed in the neutron data, even for the sample containing the smallest amount of Ti and second-neighbour correlations are more clearly observed from the x-ray data. The presence of only a small amount of Ti is sufficient to cause a significant narrowing of the Si–O bondlength distribution, which is intimately related to the macroscopic structural changes associated with the addition of Ti. For the pure silica gel, the gel-forming reactions proceed slowly enough to allow the formation of voids within the network, the surfaces of which are lined with –OH groups, terminating the network. The addition of Ti catalyses condensation reactions, eliminating larger voids from the bulk structure. In this case, some –OH groups remain as network defects, however we conclude that most lie on surfaces at the edges of strained but otherwise homogeneous network regions. For the 41 mol% titania sample, this effect has increased to the extent that –OH groups form the barrier between the two phases. There is evidence from the more novel shallow-angle-of-incidence measurements for a higher degree of disorder in the silica network of the thin films, with a reduction in the number of Si–O–Si chains relative to Si–O bonds when compared to the bulk.

Titanium has a important role to play in the preparation of these materials, not primarily as a network modifier, but as a catalyst for condensation reactions. Its effects on the macroscopic structure highlight the need to consider the network-terminating/modifying effect of –OH bonds when producing a model structure. From the experimental data presented here, it is clear that the structure of these materials can only be understood if the role of hydrogen is also included in any discussion; additional experimental (diffraction, inelastic scattering, SAXS, EXAFS, masNMR and IR spectroscopy) and computer modelling work is underway.

Acknowledgments

The work reported here was financially supported by the EPSRC and the University of Kent at Canterbury; JKW acknowledges the support of the Royal 1851 Commission.

References

[1] Brinker C J and Scherer G W 1990 *Sol-gel Science: the Physics and Chemistry of Sol-gel Processing* (San Diego, CA: Academic)
[2] Itoh M, Hattori H and Tanabe K J 1974 *J. Catalysis* **35** 225
[3] Smith M E and Whitfield H J 1994 *J. Chem. Soc., Chem. Comm.* **6** 723
[4] Dirken P J, Smith M E and Whitfield H J 1995 *J. Phys. Chem.* **99** 395.
[5] Bastow T J, Moodie A F, Smith M E and Whitfield H J 1993 *J. Mater. Chem.* **3** 697
[6] Cheng J-J and Wang D-W 1988 *J. Non-Crystal Solids* **100** 288
[7] Emili M, Incoccia L, Mobilio S, Fagherazzi G and Guglielmi M 1985 *J. Non-Crystal Solids* **74** 129
[8] Rigden J S, Newport R J, Smith M E, Dirken P J and Bushnell-Wye G 1996 *J Mater. Chem.* **6** 337
Walters J K, Rigden J S, Dirken P J, Smith M E, Howells W S and Newport R J 1997 *Chem Phys Lett.* **264** 539
[9] Dirken P J, Dupree R and Smith M E 1995 *J Mater. Chem.* **5** 1261
[10] Bornside D E, Macosko C W and Scriven L E 1987 *J. Imag. Technol.* **13** 122
[11] Boland B and Whapham S (eds) 1992 *ISIS Experimental Facilities* (Rutherford Appleton Laboratory)

[12] Cusack N E 1987 *The Physics of Structurally Disordered Matter* (Bristol: Hilger)
Newport R J 1988 *Neutron Scattering at a Pulsed Source* ed R J Newport, B D Rainford and R Cywinski (Bristol: Hilger)
[13] Soper A K, Howells W S and Hannon A C 1989 *Rutherford Appleton Laboratory Report* RAL-89-046
[14] Walters J K, Honeybone P J R, Huxley D W, Newport R J and Howells W S 1994 *Phys. Rev.* B **50** 831
[15] Lim W P G and Ortiz C 1987 *J. Mater. Res.* **2** 471
[16] Burke T M, Huxley D W, Newport R J and Cernik R 1992 *Rev. Sci. Instrum.* **63** 1150
Burke T M 1994 An x-ray and neutron diffraction study of amorphous hydrogenated carbon *PhD Thesis* University of Kent at Canterbury
[17] Bushnell-Wye G and Cernik R 1992 *Rev. Sci. Instrum.* **63** 999
[18] Huxley D W 1991 Diffraction studies of amorphous materials *PhD Thesis* University of Kent at Canterbury
[19] Warren B E 1990 *X-ray Diffraction* (New York: Dover)
[20] Macgillavry C H and Rieck G D (eds) 1968 *International Tables of X-ray Crystallography* vol III (Kynoch Press for International Union of Crystallography)
[21] Waser J 1953 *Rev. Mod. Phys.* **25** 671
[22] Loshmanov A A, Sigaev V N and Yamzin I I 1974 *Sov. Phys. Cryst.* **19** 168
[23] Sandstrom D R, Lytle F W, Wei P S P, Greegor R B, Wong J and Schultz P 1980 *J. Non-Crystal Solids* **41** 201
[24] Duran A, Serna C, Fornes V and Fernandez Navarro J M 1986 *J. Non-Crystal Solids* **82** 69
[25] Scharml-Marth M, Walther K L, Wokaun A, Handy B E and Baiker A 1992 *J. Non-Crystal Solids* **143** 93